Thermal Science and Engineering 2024, 7(1), 5949.
https://doi.org/10.24294/tse.v7i1.5949

Article

Theoretical investigation on diastereoselective [2+2] cycloaddition and Pd-catalyzed enantioselective [3+2] cycloaddition for synthesis of cis-β-lactam and exo-furobenzopyranone

Nan Lu*, Chengxia Miao, Xiaozheng Lan

College of Chemistry and Material Science, Shandong Agricultural University, Taian 271018, China
*** Corresponding author:** Nan Lu, lun@sdau.edu.cn

CITATION

Lu N, Miao V, Lan X. Theoretical investigation on diastereoselective [2+2] cycloaddition and Pd-catalyzed enantioselective [3+2] cycloaddition for synthesis of cis-β-lactam and exo-furobenzopyranone. Thermal Science and Engineering. 2024; 7(1): 5949. https://doi.org/10.24294/tse.v7i1.5949

ARTICLE INFO

Received: 22 April 2024
Accepted: 17 May 2024
Available online: 25 June 2024

Abstract: The mechanism is investigated for Wolff rearrangement/Staudinger [2+2] cycloaddition cascade and Pd-catalyzed, decarboxylative, formal [3+2] cycloaddition. Wolff rearrangement of 3-diazotetramic acid is determined to be rate-limiting step generates cyclic acyl ketene. The interaction of ketene with imine firstly results in zwitterion followed by conrotatory cyclization giving major cis-β-lactam. For synthesis of s-VECs, the epoxidation−cyclization cascade and hydrolysis give precursor of better performing exocyclic derivative. The reaction with 3-cyanochromone includes decarboxylation, nucleophilic attack and subsequent ring closure yielding 5-exo-trig furobenzopyranone. Based on the comparison between possible paths, the diastereoselectivity of cis over trans and regio-divergence of 5-exo-trig over 7-endo-trig are both kinetically controlled for [2+2] and [3+2] cycloaddition in common. The positive solvation effect is suggested by decreased absolute and activation energies in chlorobenzene and chloroform solution compared with in gas. These results are supported by Multiwfn analysis on FMO composition of specific TSs, and MBO value of vital bonding, breaking.

Keywords: cycloaddition; diastereoselective; enantioselective; wolff rearrangement; spirocyclic scaffold

1. Introduction

As an important component of modern drug design, new heterocyclic scaffold possess attractive physical and biological profile from medicinal chemistry perspective. Among these unexplored molecular frameworks, the some spirocyclic structures are the most sought-after motifs [1]. The β-Lactam also known as 2-azetidinone is privileged and well established in medicinal chemistry [2,3]. Thus convenient methods for synthesis of β-lactam have attracted considerable attention with available substitution pattern. A highly worthy goal is to develop efficient synthetic methodology toward spirocyclic β-lactam frame-works. Although there is cascade Wolff rearrangement/Staudinger [2+2] cycloaddition as an active and powerful tool to produce β-lactam [4,5], few examples have been reported using cyclic diazo compound in construction of spirocyclic β-lactam [6,7]. In this field of assembling pirocyclic scaffold based on diazo heterocycle transformation, Dar'in group have achieved many good results through exploring diazo tetramic acid [8–10].

On the other, organic carbonates (OCs) especially cyclic OCs are widely used as chemical synthons and can be prepared from various organocatalytic methods [11]. As precursor of zwitterionic oxa-Pd−allyl complex upon decarboxylation, vinyl

ethylene carbonates (VECs) resemble versatile OCs in cycloaddition with electrophiles. Many pioneering works have been published. Khan reported an efficient method for construction of furanobenzodihydropyran through Pd-catalyzed asymmetric decarboxylative cycloaddition of vinylethylene carbonates with 3-cyanochromones [12]. Shah enabled enantioselective synthesis of 2,3-dihydrofurans bearing quaternary stereocenter via Pd-catalyzed asymmetric cascade allylic cycloaddition and retro-Dieckmann Fragmentation [13]. Then numerous electrophiles appeared such as iso(thio)-cyanate in formal [3+2] cycloaddition for synthesis of 1,3-oxazolidine-2-thione [14], 2-arylidene-1,3-indandione in asymmetric [3+2] cycloaddition to form tetrahydrofuran-fused spirocyclic 1,3-indandione [15], isatin in decarboxylative [3+2] cycloaddition to generate functionalized spirooxindole [16], and methyleneindolinone in assembly of structurally diverse 3,3′-tetrahydrofuryl spirooxindole [17]. In another interesting direction of endo- and exo-spirocyclic VECs (s-VECs) by Schreiner group [18], the derivatization is abide by the rule of 5-exo-trig cyclization over 7-endo-trig one [19]. The excellent regio-, and enantioselectivities in Pd0-catalyzed [3+2] spiroannulation could be dominated by fine-tuning the Pd-π-allyl intermediate [20].

Many advantages have been shown for Wolff rearrangement under microwave irradiation in ring expansion of aziridine [21]. Furthermore, 3-diazotetramic acid has been successfully involved in approach toward Δα,β-spirobutenolide via Rh(II)-catalyzed O–H insertion into propiolic acid and Rh(II)-catalyzed condensation with nitriles delivering compound bearing a hitherto polysubstituted oxazole [22,23]. A new breakthrough was Dar'in's Wolff rearrangement/Staudinger [2+2] cycloaddition cascade to access spiro bis-β-lactam involving 3-diazotetramic acid and imine [24]. Another one compared this was Schreiner's Pd-catalyzed, decarboxylative, formal [3+2] cycloaddition of newly synthesized s-VECs with 3-cyanochromone [25]. Although high diastereoselectivity was achieved for bis-β-lactam and excellent selectivity was provided for s-VECs synthesis, follow-up applicability, there is no report about detailed mechanistic study explaining the origin of selective cycloaddition. How three stereocenters were controlled simultaneously for novel spirocyclic bis-β-lactam? What's the mechanism of epoxidation−cyclization cascade making following exocyclic derivative overall better than endocyclic sone? To solve these mechanic problems in experiment, an in-depth theoretical study was necessary for this strategy leading to novel spiro and polyspiro heterocyclic structure with two different isomers.

2. Computational details

The geometry optimizations were performed at the B3LYP/BSI level with the Gaussian 09 package [26,27]. The mixed basis set of LanL2DZ for Pd and 6–31G(d) for non-metal atoms [28–32] was denoted as BSI. Different singlet and multiplet states were clarified with B3LYP and ROB3LYP approaches including Becke's three-parameter hybrid functional combined with Lee−Yang−Parr correction for correlation [33–39]. The nature of each structure was verified by performing harmonic vibrational frequency calculations. Intrinsic reaction coordinate (IRC)

calculations were examined to confirm the right connections among key transition-states and corresponding reactants and products. Harmonic frequency calculations were carried out at the B3LYP/BSI level to gain zero-point vibrational energy (ZPVE) and thermodynamic corrections at 473 K, 363 K and 1 atm for each structure in chlorobenzene and chloroform. The solvation-corrected free energies were obtained at the B3LYP/6-311++G(d,p) (LanL2DZ for Pd) level by using integral equation formalism polarizable continuum model (IEFPCM) in Truhlar's "density" solvation model [40–42] on the B3LYP/BSI-optimized geometries.

As an efficient method of obtaining bond and lone pair of a molecule from modern ab initio wave functions, NBO procedure was performed with Natural bond orbital (NBO3.1) to characterize electronic properties and bonding orbital interactions [43,44]. The wave function analysis was provided using Multiwfn_3.7_dev package [45] including research on frontier molecular orbital (FMO) and Mayer bond order (MBO).

3. Results and discussion

The mechanism was explored for (a) reaction of 3-diazotetramic acid 1 with imine 2 leading to spiro bis-β-lactam 3 (b) synthesis of s-VECs exo-6 and endo-4 and Pd-catalyzed, decarboxylative-[3+2] cycloaddition with 3-cyanochromone 9 producing furobenzopyranone 10, 11 (**Scheme 1**). Illustrated by black arrow of **Scheme 2a**, Wolff rearrangement of 1 forms vital cyclic acyl ketene A, which proceeds [2+2] cycloaddition with 2 involving two steps. The interaction of ketene with 2 firstly results in β-lactam zwitterionic intermediate zi3 followed by ring closure and subsequent conrotatory cyclization giving major "cis" product denoted as c3. Shown by black arrow of **Scheme 2b**, the epoxidation−cyclization cascade of cyclic allylic alcohol initially gives an iminium ion intermediate 8, which is hydrolyzed in the following two steps affording carbonate. Promoted by model catalyst $PdCl_2$, the decarboxylation intermediate of better performing exo-6 is obtained in the beginning, whose nucleophilic attack on 9 and subsequent ring closure completing [3+2] cycloaddition. The schematic structures of optimized TSs in **Scheme 2** are listed in **Figure 1**. The activation energy was shown in **Table 1** for all steps. Supplementary **Table S15**, **Table S16** provided the relative energies of all stationary points. According to experiment, the Gibbs free energies in chlorobenzene and chloroform solution phase are discussed here.

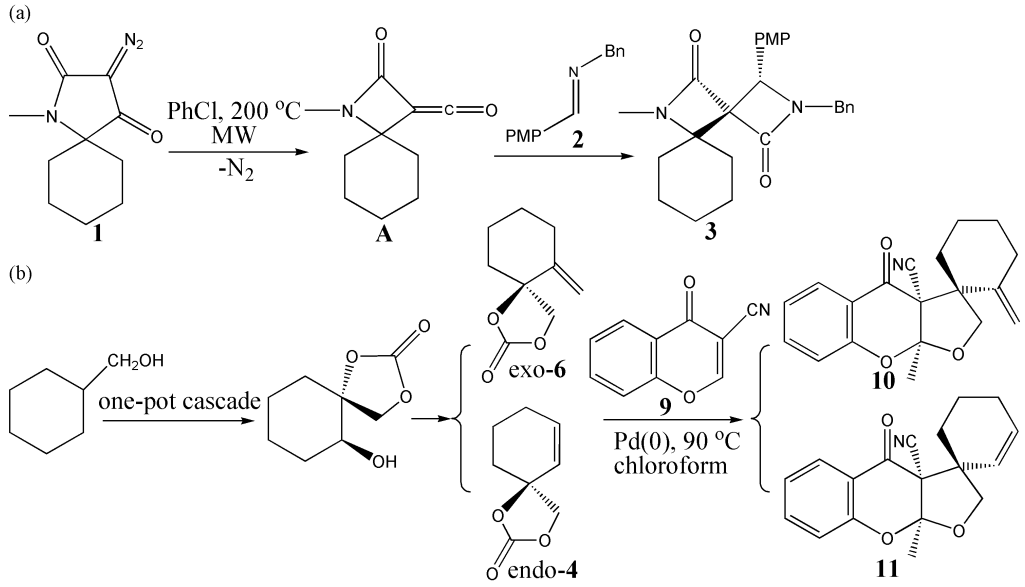

Scheme 1. (a) Thermally promoted reaction of 3-diazotetramic acid 1 with imine 2 leading to spiro bis-*β*-lactam 3; **(b)** synthesis of exo- and endo-spirovinylethylene carbonates (s-VECs) 6, 4 from cyclic allylic alcohol and Pd-catalyzed, decarboxylative-[3+2] cycloaddition with 3-cyanochromone 9 producing furobenzopyranone 10, 11.

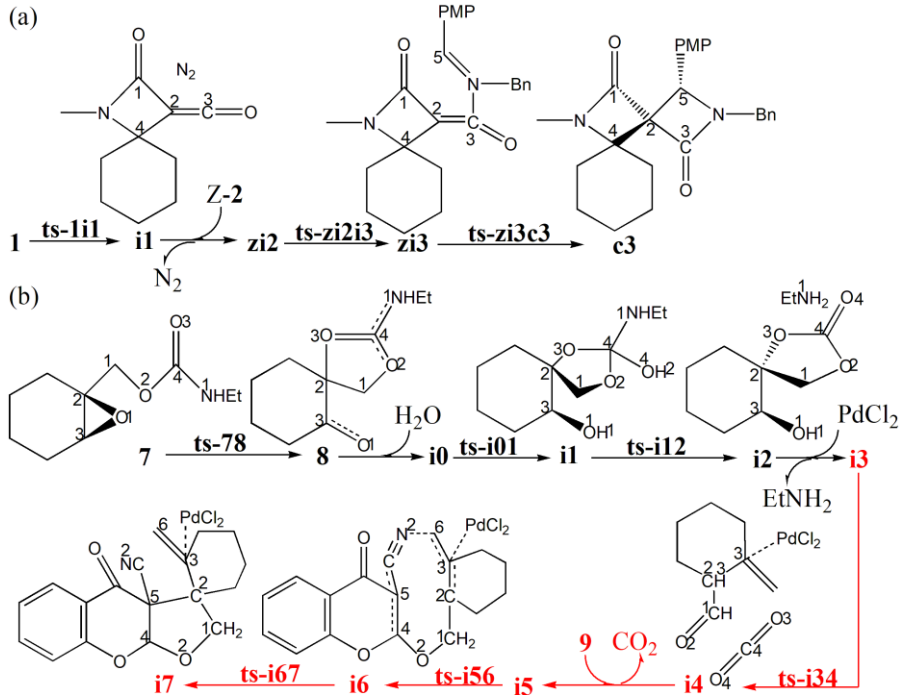

Scheme 2. Proposed reaction mechanism of **(a)** 1 with Z-2 leading to major cis isomer c3; **(b)** epoxidation−cyclization forming spirocyclic carbonate; exo-6 with 9 producing 10. TS is named according to the two intermediates it connects.

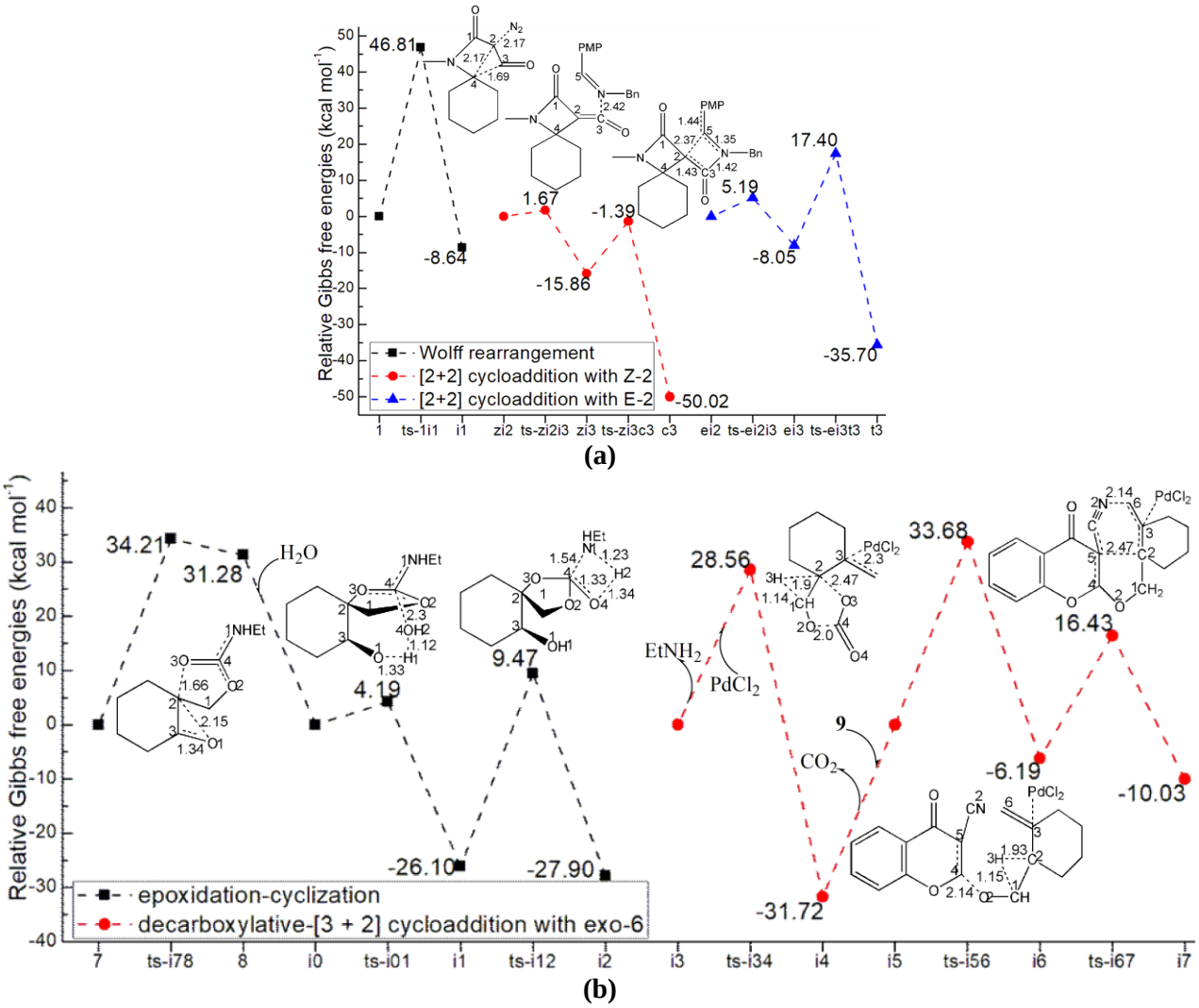

Figure 1. Relative Gibbs free energy profile in solvent phase starting from complex **(a)** 1, zi2, ei2; **(b)** 7, i0, i3, i5 (Bond lengths of optimized TSs in Å).

Table 1 The activation energy (in kcal mol^{-1}) of all reactions in gas and solvent.

TS	$\Delta G^{\neq}_{gas}$	$\Delta G^{\neq}_{sol}$
ts-1i1	46.07	46.81
ts-zi2i3	2.11	1.67
ts-zi3c3	14.76	14.48
ts-ei2i3	5.31	5.19
ts-ei3t3	22.17	25.45
ts-i78	48.02	34.21
ts-i01	2.74	4.20
ts-i12	34.72	35.57
ts-i34	29.79	28.56
ts-i56	35.04	33.68
ts-i67	23.39	22.61
4-ts-i34	32.38	29.20
4-ts-i56	39.83	36.95
4-ts-i67	26.29	23.86

3.1. Wolff rearrangement/Staudinger [2+2] cycloaddition cascade

Wolff rearrangement proceeds via ts-1i1 as step 1 with the activation energy of 46.8 kcal mol^{-1} relative to the starting point 1 (black dash line of **Figure 1a**). The transition vector of ts-1i1 includes the cleavage of C2-N, C3-C4 bond and closing of C2 to C4 slightly later (1.69, 2.17, 2.17 Å) (**Figure S1a**). Once N_2 leaves from the system, the five-membered ring of 1 turns to be four-membered one, which is the stable vital cyclic acyl ketene A in resultant i1 exothermic by −8.6 kcal mol^{-1}. The barrier is somewhat high yet still feasible to overcome considering the high temperature of 200 ℃ under microwave irradiation in experiment.

In the following [2+2] cycloaddition, although *E* form of imine 2 is predominating with lower relative energy, *Z*-2 is selected to discuss the mechanism owing to the same process and the final major "cis" product. The initial complex binding A and *Z*-2 denoted as zi2 is taken as the starting point of next two steps. The nucleophilic attack of *Z*-2 to A occurs via ts-zi2i3 with activation energy of 1.7 kcal mol^{-1} rather small (red dash line of **Figure 1a**) leading to zwitterionic intermediate zi3 continuously exothermic by −15.9 kcal mol^{-1}. The transition vector is simple corresponding to the N···C3 bonding (2.42 Å) (**Figure S1b**).

The intr**o**duction of strongly electron-donating p-methoxyphenyl (PMP) and benzyl (Bn) at iminium moiety disfavor direct ring closure. Thereby step 3 is required to complete fast conrotatory cyclization from diastereomeric zwitterion, which takes place via ts-zi3c3 with activation energy of 14.5 kcal mol^{-1} and huge heat release of −50.0 kcal mol^{-1}furnishing a new four-membered ring with an intersection arrangement of the previous one in final c3. The transition vector contains the approaching of C2 to C5 and concert elongation of N-C5, C2-C3 double bond to single one (2.37, 1.35, 1.43 Å) (**Figure S1c**). The latter two steps are both readily accessible with low activation energy from kinetics and quite favorable from thermodynamics. Thus Wolff rearrangement is determined to be rate-limiting of the whole reaction.

3.2. Epoxidation−cyclization cascade

Shown by black dash line of **Figure 1b**, the epoxidation structure of cyclic allylic alcohol 7 is located and taken as starting point of epoxidation−cyclization cascade, from which the cyclization initiated from negative carbonyl O3 to epoxane positive C2 takes place via ts-i78 with activation energy of 34.2 kcal mol^{-1} endoergic by 31.3 kcal mol^{-1} affording an iminium ion intermediate 8 in step 1. The transition vector also includes the breaking of C2-O1 and shortening of C1-O3 single bond (1.66, 2.15, 1.34 Å) (**Figure S1d**). The destruction of epoxy structure makes the negative charge significantly transferred to epoxy O1.

With water molecule, the reactive 8 is prone to be hydrolyzed through the following two steps affording carbonate in i2. The new starting point between 8 and H_2O is located as i0, from which the protonation of negative O1 is readily to undergo via ts-i01 with activation energy of 4.2 kcal mol^{-1} exothermic by −26.1 kcal mol^{-1} in step 2. In addition to the obvious indication of H1 shift from O4 of H_2O to O1, the transition vector also indicates asynchronous O4 bonding to C4 (1.12, 1.33, 2.3 Å) (**Figure S1e**). The resultant i1 is stable with pronated O1H1 and sp3 hybrid C4.

Another H2 of H_2O is provided to N1 in step 3 (1.34, 1.23 Å) via ts-i12 with the activation energy of 35.6 kcal mol^{-1} relative to i1. Meanwhile C4-O4 single bond is contracted to double one and the dissociation of N1 from C4 causes depature of $EtNH_2$ molecule (1.33, 1.54 Å) in stable i2. This detailed motion can be demonstrated by the transition vector of ts-i12 (**Figure S1f**). Thankfully, this step is continuously exothermic by −27.9 kcal mol^{-1} favorable thermodynamically. The barriers of step 1 and step 3 somewhat high are both capable to overcome under the experimental temperature of 90 ℃.

3.3. Pd(0)-catalyzed decarboxylative [3+2] cycloaddition

Two types of s-VEC exo-6 and endo-4 are obtained from carbonate i2, the interaction of better performing exo-6 with Pd(0) is discussed in detail. The decarboxylation happens via ts-i34 in step 4 with a barrier of 28.6 kcal mol^{-1} relative to starting point i3 exothermic by −31.7 kcal mol^{-1} yielding i4 a stable aldehyde structure. The transition vector is composed of remarkable O2⋯C4 and C2⋯O3 fracture and laggering proton transfer C1⋯H3⋯C2 (2.0, 2.47, 1.14, 1.9 Å). The O3-C4-O4 is expanded to 180° indicating the production of CO_2 (**Figure S1g**).

The complex binding 9 denoted as i5 is taken as starting point of the following two steps completing [3+2] cycloaddition. According to the transition vector (**Figure S1h**), the nucleophilic attack of negative aldehyde O2 to positive C4 of 9 (2.14 Å) proceeds via ts-i56 with the activation energy of 33.7 kcal mol^{-1} forming i6 exothermic by −6.2 kcal mol^{-1} in step 5. Prior to this major motion, H3 returns from C2 to C1 (1.93, 1.15 Å). It is noted that the N2-C6 bonding between cyano and terminal alkene of exo-6 favorable for stabilizing is not available for endo-4, making subsequent 5-exo-trig ring closure outcompetes 7-endo-trig one.

The five-membered ring is generated via ts-i67 with a barrier of 22.6 kcal mol^{-1} through concerted N2-C6 departure and C2-C5 linkage (2.14, 2.47 Å) (**Figure S1i**) liberating final i7 exothermic by -10.0 kcal mol^{-1} with recovered formal cyano and terminal alkene. $PdCl_2$ is still bonded to negative C3 of C3-C6 double bond as the promotion of whole process. Three barriers from step 4 to step 6 are mediated in agreement with requisite slightly high temperature of 90 ℃.

3.4. Diastereoselectivity and regio-divergence

To highlight the idea of feasibility for changes in electron density and not molecular orbital interactions are responsible of the reactivity of organic molecules, quantum chemical tool Multiwfn was applied to analyze of electron density such as MBO results of bonding atoms and contribution of atomic orbital to HOMO of typical TSs (**Table S17** and **S18, Figure S2**). These results all confirm the above analysis.

To explore the diastereoselectivity of Staudinger [2+2] cycloaddition, the reaction involving *E*-imine yielding *trans* isomer of bis-β-lactam is also investigated (blue dash line of **Figure 1a**) in contrast with dominant paths (red dash line). The barriers of step 1 via ts-ei2i3 and step 2 via ts-ei3t3 (5.2, 25.5 kcal mol^{-1}) are both higher than the case of ts-zi2i3 and ts-zi3c3. The regio-divergence of Pd-catalyzed, decarboxylative-[3+2] cycloaddition is explored for the latter three steps involving

endo-4 via 4-ts-i34, 4-ts-i56 and 4-ts-i67 (29.2, 37.0, 23.9 kcal mol^{-1}) also higher than those of ts-i34, ts-i56 and ts-i67. Hence the diastereoselectivity and region-selectivity puzzled in experiment are both kinetically controlled for [2+2] and [3+2] cycloaddition in common.

4. Conclusions

Our DFT calculations provide the first theoretical investigation on Wolff rearrangement/Staudinger [2+2] cycloaddition cascade and Pd-catalyzed, decarboxylative, formal [3+2] cycloaddition. Wolff rearrangement of 3-diazotetramic acid is rate-limiting step generates cyclic acyl ketene. The interaction of ketene with imine firstly results in zwitterion followed by conrotatory cyclization giving major cis-β-lactam. For synthesis of s-VECs, the epoxidation−cyclization cascade and hydrolysis give precursor of better performing exocyclic derivative. The reaction with 3-cyanochromone includes decarboxylation, nucleophilic attack and subsequent ring closure yielding 5-exo-trig furobenzopyranone. Based on the comparison between possible paths, the diastereoselectivity of cis over trans and regio-divergence of 5-exo-trig over 7-endo-trig are both kinetically controlled for [2+2] and [3+2] cycloaddition in common. The positive solvation effect is suggested by decreased absolute and activation energies in chlorobenzene and chloroform solution compared with in gas. These results are supported by Multiwfn analysis on FMO composition of specific TSs, and MBO value of vital bonding, breaking.

Supplementary materials: Supplementary data available: [Computation information and cartesian coordinates of stationary points; Calculated relative energies for the ZPE-corrected Gibbs free energies (ΔG_{gas}), and Gibbs free energies (ΔG_{sol}) for all species in solution phase at 473 K, 363 K.].

Author contributions: Conceptualization, NL; methodology, NL; software, NL; validation, NL; formal analysis, NL; investigation, NL; resources, NL; data curation, NL; writing—original draft preparation, NL; writing—review and editing, NL; visualization, NL; supervision, CM; project administration, CM; funding acquisition, XL. All authors have read and agreed to the published version of the manuscript.

Funding: This work was supported by National Natural Science Foundation of China (21973056, 21972079) and Natural Science Foundation of Shandong Province (ZR2019MB050) and Key Laboratory of Agricultural Film Application of Ministry of Agriculture and Rural Affairs, P.R. China.

Conflict of interest: The authors declare no conflict of interest.

References

1. Hiesinger K, Dar'in D, Proschak E, et al. Spirocyclic Scaffolds in Medicinal Chemistry. Journal of Medicinal Chemistry. 2020; 64(1): 150-183. doi: 10.1021/acs.jmedchem.0c01473
2. Lima LM, Silva BNM da, Barbosa G, et al. β-lactam antibiotics: An overview from a medicinal chemistry perspective. European Journal of Medicinal Chemistry. 2020; 208: 112829. doi: 10.1016/j.ejmech.2020.112829
3. Fu DJ, Zhang YF, Chang AQ, et al. β-Lactams as promising anticancer agents: Molecular hybrids, structure activity

relationships and potential targets. European Journal of Medicinal Chemistry. 2020; 201: 112510. doi: 10.1016/j.ejmech.2020.112510
4. Chen L, Wang K, Shao Y, et al. Stereoselective Synthesis of Fully Substituted β-Lactams via Metal–Organo Relay Catalysis. Organic Letters. 2019; 21(10): 3804-3807. doi: 10.1021/acs.orglett.9b01255
5. Krasavin M, Synofzik J, Bakulina O, et al. Dialkyl Diazomalonates in Transition-Metal-Free, Thermally Promoted, Diastereoselective Wolff β-Lactam Synthesis. Synlett. 2020; 31(13): 1273-1276. doi: 10.1055/s-0040-1707811
6. Golubev AA, Smetanin IA, Agafonova AV, et al. [2+1+1] Assembly of spiro β-lactams by Rh(ii)-catalyzed reaction of diazocarbonyl compounds with azirines/isoxazoles. Organic & Biomolecular Chemistry. 2019; 17(28): 6821-6830. doi: 10.1039/c9ob01301f
7. Tang J, Yan ZH, Zhan G, et al. Visible-light-mediated sequential Wolff rearrangement and Staudinger cycloaddition enabling the assembly of spiro-pyrazolone-β-lactams. Organic Chemistry Frontiers. 2022; 9(16): 4341-4346. doi: 10.1039/d2qo00742h
8. Krasavin M, Eremeyeva M, Zhukovsky D, et al. The Use of α-Diazo-γ-butyrolactams in the Büchner–Curtius–Schlotterbeck Reaction of Cyclic Ketones Opens New Entry to Spirocyclic Pyrrolidones. Synlett. 2020; 31(10): 982-986. doi: 10.1055/s-0040-1708011
9. Dar'in D, Kantin G, Bakulina O, et al. Spirocyclizations Involving Oxonium Ylides Derived from Cyclic α-Diazocarbonyl Compounds: An Entry into 6-Oxa-2-azaspiro[4.5]decane Scaffold. The Journal of Organic Chemistry. 2020; 85(23): 15586-15599. doi: 10.1021/acs.joc.0c02356
10. Dar'in D, Kantin G, Chupakhin E, et al. Natural-Like Spirocyclic Δα,β-Butenolides Obtained from Diazo Homophthalimides. Chemistry – A European Journal. 2021; 27(31): 8221-8227. doi: 10.1002/chem.202100880
11. Qiao C, Villar-Yanez A, Sprachmann J, et al. Organocatalytic Trapping of Elusive Carbon Dioxide Based Heterocycles by a Kinetically Controlled Cascade Process. Angewandte Chemie International Edition. 2020; 59(42): 18446-18451. doi: 10.1002/anie.202007350
12. Khan I, Zhao C, Zhang YJ. Pd-Catalyzed asymmetric decarboxylative cycloaddition of vinylethylene carbonates with 3-cyanochromones. Chemical Communications. 2018; 54(37): 4708-4711. doi: 10.1039/c8cc02456a
13. Shah BH, Khan S, Zhao C, et al. Synthesis of Chiral 2,3-Dihydrofurans via One-Pot Pd-Catalyzed Asymmetric Allylic Cycloaddition and a Retro-Dieckmann Fragmentation Cascade. The Journal of Organic Chemistry. 2023; 88(16): 12100-12104. doi: 10.1021/acs.joc.3c00976
14. Xiong W, Zhang S, Li H, et al. Pd-Catalyzed Decarboxylative Cycloaddition of Vinylethylene Carbonates with Isothiocyanates. The Journal of Organic Chemistry. 2020; 85(14): 8773-8779. doi: 10.1021/acs.joc.0c00243
15. Zhang H, Gao X, Jiang F, et al. Palladium-Catalyzed Asymmetric [3+2] Cycloaddition of Vinylethylene Carbonates with 2-Arylidene-1,3-Indandiones: Synthesis of Tetrahydrofuran-Fused Spirocyclic 1,3-Indandiones. European Journal of Organic Chemistry. 2020; 2020(30): 4801-4804. doi: 10.1002/ejoc.202000762
16. Li T, Zhu X, Jiang H, et al. Pd-catalyzed decarboxylative [3 + 2] cycloaddition: Assembly of highly functionalized spirooxindoles bearing two quaternary centers. Applied Organometallic Chemistry. 2021; 36(2). doi: 10.1002/aoc.6516
17. Wang J, Zhao L, Rong Q, et al. Asymmetric Synthesis of 3,3′-Tetrahydrofuryl Spirooxindoles via Palladium-Catalyzed [3+2] Cycloadditions of Methyleneindolinones with Vinylethylene Carbonates. Organic Letters. 2020; 22(15): 5833-5838. doi: 10.1021/acs.orglett.0c01920
18. Reis J, Gaspar A, Milhazes N, et al. Chromone as a Privileged Scaffold in Drug Discovery: Recent Advances. Journal of Medicinal Chemistry. 2017; 60(19): 7941-7957. doi: 10.1021/acs.jmedchem.6b01720
19. Gilmore K, Alabugin IV. Cyclizations of Alkynes: Revisiting Baldwin's Rules for Ring Closure. Chemical Reviews. 2011; 111(11): 6513-6556. doi: 10.1021/cr200164y
20. Trost BM, Zuo Z. Regiodivergent Synthesis of Spirocyclic Compounds through Pd-Catalyzed Regio- and Enantioselective [3+2] Spiroannulation. Angewandte Chemie International Edition. 2021; 60(11): 5806-5810. doi: 10.1002/anie.202016439
21. Lei Y, Xu J. Efficient synthesis of ethyl 2-(oxazolin-2-yl)alkanoates via ethoxycarbonylketene-induced electrophilic ring expansion of aziridines. Beilstein Journal of Organic Chemistry. 2022; 18: 70-76. doi: 10.3762/bjoc.18.6
22. Darin D, Kantin G, Glushakova D, et al. Diazo Tetramic Acids Provide Access to Natu-ral-Like Spirocyclic Δα,β-Butenolides through Rh(II)-Catalyzed O-H Insertion/Base-Promoted Cyclization. The Journal of Organic Chemistry. 2023; doi: 10.1021/acs.-joc.2c02600
23. Krivovicheva V, Kantin G, Dar'in D, et al. Rh(II)-catalyzed condensation of 3-diazotetramic acids with nitriles delivers

novel druglike 5,6-dihydro-4H-pyrrolo[3,4-d]oxazol-4-ones. Tetrahedron Letters. 2023; 120: 154457. doi: 10.1016/j.tetlet.2023.154457
24. Krivovicheva V, Lyutin I, Kantin G, et al. Access to Spiro Bis-β-lactams via a Metal-Free Microwave-Assisted Wolff Rearrangement/Staudinger [2+2] Cycloaddition Cascade Involving 3-Diazotetramic Acids and Imines. The Journal of Organic Chemistry. 2024; 89(5): 3585-3589. doi: 10.1021/acs.joc.3c02494
25. Topp C, Metzler JM, Dressler F, et al. Preparation of Spirocyclic Vinylic Carbonates from Allylic Alcohols. Organic Letters. 2024; 26(3): 577-580. doi: 10.1021/acs.orglett.3c03253
26. Frisch MJ, Trucks GW, Schlegel HB, et al. Gaussian 09 (Revision B.01). Gaussian, Inc., Wallingford; CT; 2010.
27. Hay PJ, Wadt WR. Ab initio effective core potentials for molecular calculations. Potentials for the transition metal atoms Sc to Hg. The Journal of Chemical Physics. 1985; 82(1): 270-283. doi: 10.1063/1.448799
28. Lv H, Han F, Wang N, et al. Ionic Liquid-Catalyzed C−C Bond Formation for the Synthesis of Polysubstituted Olefins. European Journal of Organic Chemistry. 2022; 2022(45). doi: 10.1002/ejoc.202201222
29. Zhuang H, Lu N, Ji N, et al. Bu4NHSO4-Catalyzed Direct N-Allylation of Pyrazole and its Derivatives with Allylic Alcohols in Water: A Metal-Free, Recyclable and Sustainable System. Advanced Synthesis & Catalysis. 2021; 363(24): 5461-5472. doi: 10.1002/adsc.202100864
30. Lu N, Lan X, Miao C, et al. Theoretical investigation on transformation of Cr(II) to Cr(V) complexes bearing tetra-N-heterocyclic carbene and group transfer reactivity. International Journal of Quantum Chemistry. 2020; 120(18). doi: 10.1002/qua.26340
31. Lu N, Liang H, Qian P, et al. Theoretical investigation on the mechanism and enantioselectivity of organocatalytic asymmetric Povarov reactions of anilines and aldehydes. International Journal of Quantum Chemistry. 2020; 121(8). doi: 10.1002/qua.26574
32. Lu N, Wang Y. Alloy and media effects on the ethanol partial oxidation catalyzed by bimetallic Pt6M (M = Co, Ni, Cu, Zn, Ru, Rh, Pd, Sn, Re, Ir, and Pt). Computational and Theoretical Chemistry. 2023; 1228: 114252. doi: 10.1016/j.comptc.2023.114252
33. Becke AD. Density-functional thermochemistry. IV. A new dynamical correlation functional and implications for exact-exchange mixing. The Journal of Chemical Physics. 1996; 104(3): 1040-1046. doi: 10.1063/1.470829
34. Lee C, Yang W, Parr RG. Development of the Colle-Salvetti correlation-energy formula into a functional of the electron density. Physical Review B. 1988; 37(2): 785-789. doi: 10.1103/physrevb.37.785
35. Catellani M, Mealli C, Motti E, et al. Palladium−Arene Interactions in Catalytic Intermediates: An Experimental and Theoretical Investigation of the Soft Rearrangement between η1 and η2 Coordination Modes. Journal of the American Chemical Society. 2002; 124(16): 4336-4346. doi: 10.1021/ja016587e
36. Zicovich-Wilson CM, Pascale F, Roetti C, et al. Calculation of the vibration frequencies of α-quartz: The effect of Hamiltonian and basis set. Journal of Computational Chemistry. 2004; 25(15): 1873-1881. doi: 10.1002/jcc.20120
37. Nielsen RJ, Goddard WA. Mechanism of the Aerobic Oxidation of Alcohols by Palladium Complexes of N-Heterocyclic Carbenes. Journal of the American Chemical Society. 2006; 128(30): 9651-9660. doi: 10.1021/ja060915z
38. Zandler ME, D'Souza F. The remarkable ability of B3LYP/3-21G(*) calculations to describe geometry, spectral and electrochemical properties of molecular and supramolecular porphyrin–fullerene conjugates. Comptes Rendus Chimie. 2006; 9(7-8): 960-981. doi: 10.1016/j.crci.2005.12.008
39. Marenich AV, Cramer CJ, Truhlar DG. Universal Solvation Model Based on Solute Electron Density and on a Continuum Model of the Solvent Defined by the Bulk Dielectric Constant and Atomic Surface Tensions. The Journal of Physical Chemistry B. 2009; 113(18): 6378-6396. doi: 10.1021/jp810292n
40. Tapia O. Solvent effect theories: Quantum and classical formalisms and their applications in chemistry and biochemistry. Journal of Mathematical Chemistry. 1992; 10(1): 139-181. doi: 10.1007/bf01169173
41. Tomasi J, Persico M. Molecular Interactions in Solution: An Overview of Methods Based on Continuous Distributions of the Solvent. Chemical Reviews. 1994; 94(7): 2027-2094. doi: 10.1021/cr00031a013
42. Tomasi J, Mennucci B, Cammi R. Quantum Mechanical Continuum Solvation Models. Chemical Reviews. 2005; 105(8): 2999-3094. doi: 10.1021/cr9904009
43. Reed AE, Weinstock RB, Weinhold F. Natural population analysis. The Journal of Chemical Physics. 1985; 83(2): 735-746. doi: 10.1063/1.449486
44. Reed AE, Curtiss LA, Weinhold F. Intermolecular interactions from a natural bond orbital, donor-acceptor viewpoint.

Chemical Reviews. 1988; 88(6): 899-926. doi: 10.1021/cr00088a005

45. Lu T, Chen F. Multiwfn: A multifunctional wavefunction analyzer. Journal of Computational Chemistry. 2011; 33(5): 580-592. doi: 10.1002/jcc.22885